Available online at www.sciencedirect.com
ScienceDirect
Journal of the European Ceramic Society 31 (2011) 1827–1833
www.elsevier.com/locate/jeurceramsoc

Fracture behavior of silicon nitride ceramics under combined compression–torsion stresses analyzed by multiaxial fracture statistics

N. Kawai *, T. Kotani, Y. Kakimoto, E. Sato

Institute of Space and Astronautical Science, Japan Aerospace Exploration Agency, 3-1-1 Yoshinodai, Chuo, Sagamihara, Kanagawa 252-5210, Japan

Received 30 September 2010; received in revised form 18 February 2011; accepted 11 March 2011
Available online 12 April 2011

Abstract

Combined compression–torsion tests were performed on the thermal-treated and as-machined silicon nitride ceramics to investigate their fracture behavior under multiaxial stress states. The thermal-treated samples showed considerable high strength and low anisotropy to the grinding direction in flexure tests compared to the as-machined samples. Under combined compression and torsion stress states, the thermal-treated samples showed considerably higher tensile strength than that of as-machined samples at low compressive stress states and weakening with increasing compression stress. The as-machined samples showed little decrease in tensile strength with increasing compression stress and comparable tensile strength with the thermal-treated samples under a highly compressive stress state. The behavior of thermal-treated samples were well described by the statistical theory of multiaxial fracture for volume-distributed flaws combined with a mixed-mode fracture criterion with the shear sensitivity constant of 1.75 and 1.65 for Shetty's criterion and the ellipsoidal criterion, respectively.

Keywords: Silicon nitride; Failure analysis; Fracture; Strength

1. Introduction

Silicon nitride ceramics, because of their outstanding high-temperature strength, creep resistance, corrosion and erosion resistances and chemical stability, are prime structural ceramics for high-temperature applications in heat engine components and heat recovery systems such as a gas turbine engine for co-generation[1] and an orbit maneuvering engine for satellite.[2] Most structural ceramic components used in high-temperature applications are subjected to multiaxial loading, including not only tension but also compression caused by thermal stresses. Therefore, it is important to understand the fracture behavior of ceramics under multiaxial loading.

Theoretical studies for fracture strength of brittle materials under multiaxial loading have been performed using fracture statistics coupled with a mixed-mode fracture criterion.[3–5] These theoretical predictions indicate a decrease in strength under the multiaxial stress condition. Especially in the tension–compression quadrant of the principal stress space, it is predicted that fracture strength considerably decreases with increasing compressive stress because of the enhanced mode II contribution to fracture.[5]

In terms of experimental approaches, a few studies have examined the fracture strength of ceramics under tension–compression loadings,[6–19] indicating a conflict of fracture behavior in these conditions. Some reports in the literature describe a slight weakening with increasing the compressive principal stress component,[6,7,13,16] but others describe strengthening.[8,9,11,14,15,17] The discrepancy of fracture behavior complicates comparisons with theoretical studies. Therefore it is important to reexamine critically an experimental study describing fracture behavior of engineering ceramics under multiaxial loading conditions.

Silicon nitride is a material on which thermal-oxidation-induced strengthening has been reported.[20–23] Although extensive oxidation engenders strength degradation, slight oxidation of the surface results in higher tensile strength because the glassy oxides smooth out the preexisting machining surface flaws. This thermal oxidation strengthening technique is commonly used for silicon nitride components. However, the effectiveness of this treatment under multiaxial loading has not been investigated yet.

* Corresponding author. Tel.: +81 50 3362 7539; fax: +81 42 759 8461.
E-mail address: nkawai@isas.jaxa.jp (N. Kawai).

0955-2219/$ – see front matter © 2011 Elsevier Ltd. All rights reserved.
doi:10.1016/j.jeurceramsoc.2011.03.017

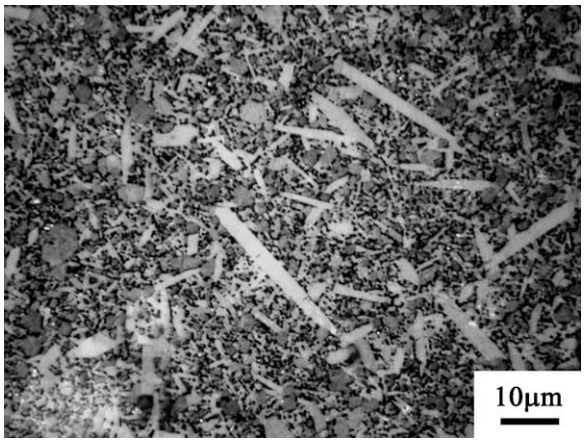

Fig. 1. Scanning electron micrograph of SN282 silicon nitride ceramics.

In this study, combined compression–torsion tests were performed on the as-machined and thermal-treated silicon nitride ceramics to investigate the fracture behavior of silicon nitride ceramics under multiaxial loading. The effectiveness of thermal treatment against finishing direction was also examined through flexure tests performed on silicon nitride ceramics ground parallel and perpendicular to the tensile axis.

2. Experimental

2.1. Material

The material used for this study is a commercially available gas-turbine grade silicon nitride, SN282 manufactured by Kyocera Corp. This silicon nitride is densified via gas-pressure sintering with Lu_2O_3 as a sintering additive and toughened with microstructures tailored to produce elongated grain structures. A scanning electron micrograph of SN282 silicon nitride ceramics is shown in Fig. 1. The bulk density is 3.38 Mg/m^3. The elastic modulus, shear modulus, and Poisson's ratio are 316 GPa, 123 GPa, and 0.28, respectively.[24]

For flexure tests, beam specimens of 3 mm × 4 mm × 40 mm were used. The specimen surface was ground using 400 grit diamond wheels. Grinding was conducted either parallel or perpendicular to the bar length, which is the tensile axis of the flexure test.

In compression–torsion tests, dumb-bell shaped specimens, shown in Fig. 2, were used. These samples were produced by grinding 4 mm × 4 mm × 20 mm square rods along the circumferential direction using 400 grit diamond wheels and by finishing using 2000 grit diamond paper. The test area has 2 mm diameter and 4 mm length. The 4-mm cubic block parts at both ends act as transmitters of a compression force and a torsional force by connecting to the test equipment.

Some machined and ground specimens were heat-treated at 1300 °C for 1 h in air. The depth profile of oxygen content was measured by the Auger electron spectroscopy, as shown in Fig. 3. The atomic percentage of oxygen was 8 % at 50 nm in depth from the sample surface for the as-machined sample; on the other hand it was 50 % from surface to 200 nm in depth and started decreasing in larger depth for the thermal-treated sample. This indicates that the silicon nitride surface was sufficiently oxidized in this heat treatment.

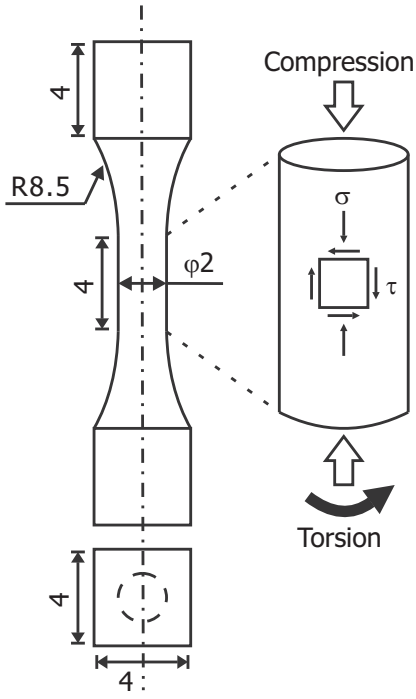

Fig. 2. Schematic of a sample used for compression–torsion testing and the stress state in combined compression and torsion loading.

2.2. Test equipment

All experiments were conducted using a universal testing machine (Autograph AG-20kNI, Shimazu Corp.) retrofitted with a torque driver and a torque cell at room temperature under atmospheric conditions. The flexure strength was measured using a four-point bend fixture with outer and inner spans of 30 and 10 mm, respectively. Flexure tests were performed at

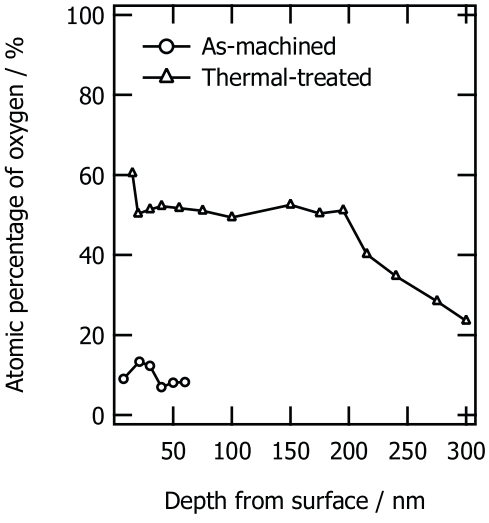

Fig. 3. Depth profile of oxygen content measured by the Auger electron spectroscopy.

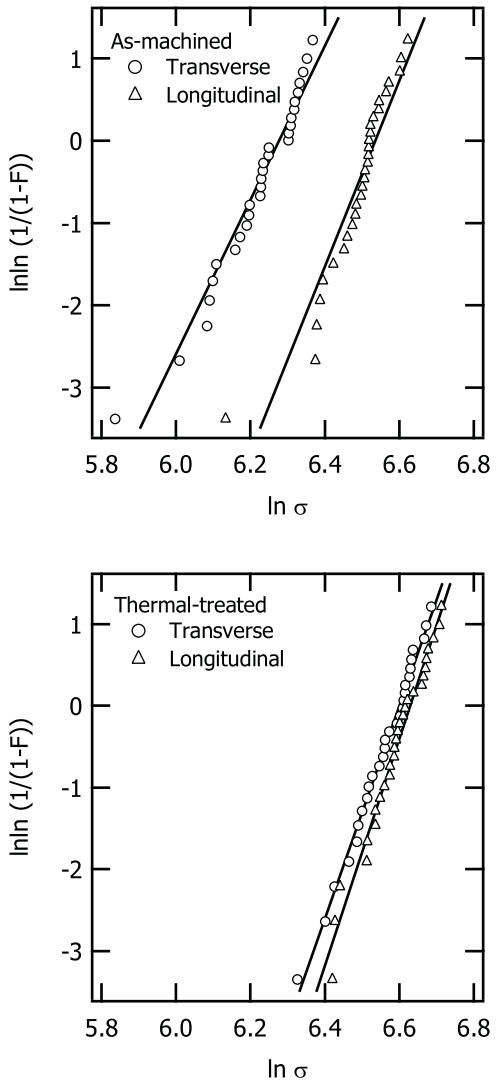

Fig. 4. Weibull distribution of flexure strength of as-machined and thermal-treated silicon nitride ground in the longitudinal and transverse directions.

a cross-head speed of 0.6 mm/min with 30 samples per condition. The compression–torsion tests were performed using the above-mentioned testing machine with a loading path as follows; first, the specimen was uniaxially compressed up to appropriate stress at a cross-head speed of 0.6 mm/min. Subsequently, it was twisted at a rotation rate of 0.01 rpm until fracture.

3. Results

3.1. Flexure tests

Weibull plots for the flexure bars ground in the longitudinal and the transverse directions are shown in Fig. 4 for the as-machined and thermal-treated samples. The fracture probability F was calculated as $F = n/(N+1)$, where n signifies the n th strength value when all strength values are placed in increasing order, and where N stands for the total number of strength measurements.

The obtained characteristic strength, σ_0, and the Weibull modulus, m, are listed for each condition in Table 1. The 90% confidence intervals[25] for each parameter are also listed. For the as-machined samples, the characteristic strength and the Weibull modulus of the transversely ground samples is lower than those of the samples ground in the longitudinal direction, which indicates that surface flaws produced by grinding become a predominant factor of fracture phenomena by acting as crack sources in these flexure tests.[26–28]

The thermal-treated samples show that the characteristic strength and the Weibull modulus of transverse ground samples are slightly less than those of longitudinal ground samples and that their strength and Weibull modulus increase compared to those of the as-machined samples. These results indicate that strength anisotropy depending on the grinding direction is eliminated by thermal oxidation.

3.2. Combined compression–torsion tests

The principal stresses under combined compression–torsion conditions are calculated using the following equations:

$$\sigma_{1,3} = \frac{\sigma}{2} \pm \left(\frac{\sigma^2}{4} + \tau^2\right)^{1/2}, \quad (1)$$

where σ_1 and σ_3 respectively denote the maximum and minimum principal stresses; σ and τ respectively signify the axial and torsional stresses. The intermediate principal stress, σ_2, is zero in this condition. The axial stress is $\sigma = P/\pi r_0^2$, where P and r_0 represent the axial load and the sample radius, respectively. The torsional stress varies with radial distance as $\tau = 2Tr/\pi r_0^4$, where T is the applied torque and r is the radial distance. At the sample surface, τ is maximum with a value of $\tau = 2T/\pi r_0^3$. To incorporate the influence of stress distribution on fracture strength in the framework of fracture statistics,[29] the measured principal stresses, $\sigma_{1,3}$, are corrected into $\sigma_{\mathrm{corr1,corr3}}$ with the effective volume, V_e, as:

$$\sigma_{\mathrm{corr1,corr3}} = \sigma_{1,3}\left(\frac{V_{e1,3}}{V_0}\right)^{1/m}, \quad (2)$$

$$V_e = 2V_0 \int_0^{r_0} \left(\frac{(\sigma/2) \pm ((\sigma^2/4) + (\tau(r/r_0))^2)^{1/2}}{(\sigma/2) \pm \left((\sigma^2/4) + \tau^2\right)^{1/2}}\right)^m r\,\mathrm{d}r. \quad (3)$$

An average value in Weibull modulus obtained by the flexure tests of longitudinal and transverse samples is conveniently used for the calculation because the angle between the principal axis and the grinding direction is between 0° and 90° and varies depending on the loading condition.

The results of the compression–torsion tests are presented in Table 2 and are shown in the principal stress space in Fig. 5. The mean flexure strengths with correction on effective volume[29] to $V_e = 4\pi$ mm^2 are also shown with values of 543 MPa for the as-machined sample and 668 MPa for the thermal-treated sample. The error bars on both strengths indicate the 90% confidence intervals calculated from the results of flexure tests. The theoretical strength envelops, of which details are described in the

Table 1
Weibull parameters obtained in four-point flexture tests. The values in parentheses indicate the 90% confidence interval.

	Longitudinal grinding		Transverse grinding	
	σ_0 (MPa)	m	σ_0 (MPa)	m
As-machined	689 (668, 711)	11 (8, 13)	532 (513, 552)	9 (7, 11)
Thermal-treated	757 (739, 776)	14 (11, 17)	735 (716, 754)	13 (10, 16)

latter session, are also drown by the solid and dashed lines in this figure.

Under low compressive stress loading, the tensile strength of the thermal-treated sample is higher than that of the as-machined sample, as shown in the results of the flexure tests. It decreases with increasing compressive stress. In contrast, the tensile strength of the as-machined sample shows just a slight decrease occurring concomitantly with increasing compressive stress. In the region where compressive stress is high, the strength of the as-machined sample is comparable to that of the thermal-treated sample. These results indicate that the influence of surface condition on the tensile strength decreases with increasing compression stress.

4. Discussion

For further understanding of the fracture behavior under multiaxial loading, comparisons of experimental results to those obtained using statistical fracture theory are performed. The probability of brittle fracture for volume-distributed penny-shaped flaws under multiaxial stress state is given as[3–5]:

$$F = 1 - \exp\left(-\int_V \left(K_s \int_A \left(\frac{\sigma_e}{\sigma_0}\right)^m dA\right) dV\right), \quad (4)$$

where σ_e signifies the effective stress given below (Eqs. (8) and (9)), V denotes a sample volume, A stands for the half surface area of unit sphere as shown in Fig. 6, and K_s is the relative coefficient[5,13] to adjust the value F of Eq. (4) to the value F of the uniaxial Weibull function:

$$F = 1 - \exp\left(-\int_V \left(\frac{\sigma}{\sigma_0}\right)^m dV\right). \quad (5)$$

In this analysis, Shetty's empirical criterion[30] and an empirical ellipsoidal criterion[31] are used as mixed-mode crack-propagation criteria because of their high applicability to various brittle materials. Shetty's criterion takes the form of:

$$\frac{K_I}{K_{Ic}} + \left(\frac{K_{II}}{K_{IIc}}\right)^2 = \frac{K_I}{K_{Ic}} + \left(\frac{K_{II}}{CK_{Ic}}\right)^2 = 1, \quad (6)$$

where K_I and K_{II} respectively represent the stress intensity factors for modes I and II, subscript c denotes the critical value, i.e. K_c being the fracture toughness, and $C = K_{IIc}/K_{Ic}$ is a shear sensitivity constant. The ellipsoidal criterion takes the form of:

$$\left(\frac{K_I}{K_{Ic}}\right)^u + \left(\frac{K_{II}}{K_{IIc}}\right)^u = \left(\frac{K_I}{K_{Ic}}\right)^u + \left(\frac{K_{II}}{CK_{Ic}}\right)^u = 1, \quad (7)$$

where u is a constant obtained empirically. In this study, u is assumed to be two as a typical value of ceramics for simplification of analysis.

The effective stress is defined as the equivalent mode I stress on the penny-shaped crack oriented in (ϕ, θ) in Fig. 6.[3,5,13,19,29,32] Using these two criteria, the effective stresses are obtained as:

$$\sigma_e = \frac{1}{2}\left(\sigma_n + \sqrt{\sigma_n^2 + \left(\frac{4\tau_p}{C(2-\nu)}\right)}\right), \quad (8)$$

Table 2
Fracture strength of silicon nitride ceramics in combined compression–torsion tests.

As-machined				Thermal-treated			
σ_1 (MPa)	σ_{corr1} (MPa)	σ_3 (MPa)	σ_{corr3} (MPa)	σ_1 (MPa)	σ_{corr1} (MPa)	σ_3 (MPa)	σ_{corr3} (MPa)
576	481	−576	−481	715	614	−715	−614
632	529	−632	−529	717	616	−717	−616
693	579	−693	−579	735	632	−735	−632
521	427	−839	−719	698	588	−1345	−1186
489	396	−1124	−985	597	501	−1553	−1390
638	517	−1594	−1403	578	483	−1860	−1684
533	428	−1806	−1623	667	557	−2262	−2054
559	449	−2156	−1955	648	540	−2402	−2191
528	422	−2759	−2551	567	471	−2802	−2596
505	402	−3373	−3162	536	444	−3083	−2879
520	414	−3388	−3172	506	418	−3373	−3173
572	456	−3438	−3204	567	470	−3432	−3213
502	399	−3688	−3475	606	502	−3472	−3242
				476	364	−3661	−3466

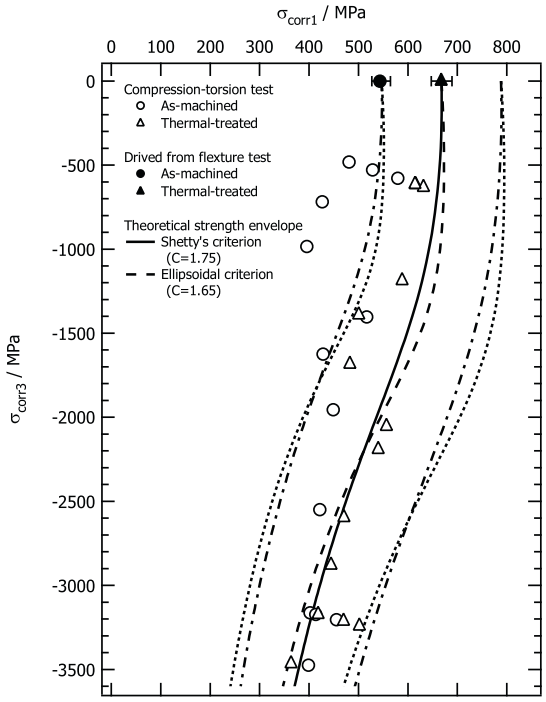

Fig. 5. Principal stresses at fracture in combined compression and torsion together with theoretical strength envelopes calculated for thermal-treated samples. Corrected principal stresses are shown as experimental results. Data for open circles and open squares were obtained from as-machined and thermal-treated samples, respectively. The mean strengths under a uniaxial stress state ($\sigma_3 = 0$) derived from the flexure strength results are shown as a solid circle for as-machined samples and as a solid square for thermal-treated samples. The error bars on the mean uniaxial strengths inidicate the 90% confidence interval. A solid line shows the theoretical strength envelope calculated using Shetty's criterion and $C = 1.75$. A dashed line shows the theoretical strength envelope calculated using the ellipsoidal criterion and $C = 1.65$. Dotted-dashed and dotted lines indicate the 95% probability band for the strength envelopes calculated using Shetty's criterion and the ellipsoidal criterion, respectively.

for Shetty's criterion, and

$$\sigma_e = \left(\sigma_n^2 + \left(\frac{\tau_p}{C\,(1-\nu/2)}\right)^2\right)^{1/2}, \tag{9}$$

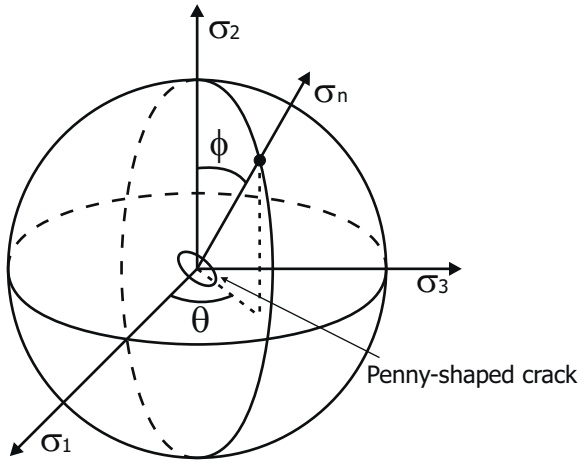

Fig. 6. Unit sphere representation of normal stress σ_n on a penny-shaped crack.

for the ellipsoidal criterion, where ν stands for Poisson's ratio, σ_n denotes the normal tensile stress on the crack plane, and τ_p signifies the shear stress applied parallel to the crack plane. Here, σ_n and τ_p are calculated as:

$$\sigma_n = \sigma_1 \sin^2\phi\cos^2\theta + \sigma_2\cos^2\phi + \sigma_3\sin^2\phi\sin^2\theta, \tag{10}$$

$$\tau_p^2 = \sigma_1^2\sin^2\phi\cos^2\theta + \sigma_2^2\cos^2\phi + \sigma_3^2\sin^2\phi\sin^2\theta - \sigma_n^2. \tag{11}$$

The relative coefficient K_s is expressed as:

$$K_s = (\pi I)^{-1}, \tag{12}$$

where

$$I = \int_0^{\pi}\left(\frac{1}{2}\left(\cos^2\phi + \sqrt{\cos^4\phi + \left(\frac{4}{C\,(2-\nu)}\right)^2\sin^2\phi\cos^2\phi}\right)\right)^m \sin\phi\,\mathrm{d}\phi, \tag{13}$$

for Shetty's criterion,

$$I = \int_0^{\pi}\left(\cos^4\phi + \left(\frac{2}{C\,(2-\nu)}\right)^2\sin^2\phi\cos^2\phi\right)^{m/2}\sin\phi\,\mathrm{d}\phi, \tag{14}$$

for the ellipsoidal criterion.

From the fundamental equation of multiaxial fracture statistics, Eq. (4), we can obtain the expected value of σ_1 at fracture under multiaxial stress states, σ_1^E, when the stress ratio $k = \sigma_3/\sigma_1$ is given:

$$\sigma_1^E(k) = \int_0^{\infty}\exp\left(-\int_V\left(K_s\int_A\left(\frac{\sigma_e}{\sigma_0}\right)^m \mathrm{d}A\right)\mathrm{d}V\right)\mathrm{d}\sigma_1$$

$$= \sigma_0 Q_s^{-1/m}\Gamma\left(1+\frac{1}{m}\right), \tag{15}$$

where Γ is the Gamma function, and

$$Q_s = \frac{2V_0}{\pi I}\int_0^D\int_0^{\pi}\left(\frac{\sigma_e}{\sigma_1}\right)^m \sin\phi\,\mathrm{d}\phi\,\mathrm{d}\theta. \tag{16}$$

The standard deviation, $\delta(k)$, of theoretical strength is given:

$$\delta(k) = \sigma_0 Q_s^{-1/m}\left(\Gamma\left(1+\frac{2}{m}\right) - \left(\Gamma\left(1+\frac{1}{m}\right)\right)^2\right)^{1/2}. \tag{17}$$

In this calculation, it is assumed that the crack to which compressive normal stress is applied does not propagate. Therefore, integration in Eq. (16) is restricted over angle θ satisfying $|\theta| < D$, where, from Eq. (10) with $\sigma_2 = 0$:

$$D = \sin^{-1}((1-k)^{-1/2}). \tag{18}$$

The fracture envelopes calculated from Eq. (15) are compared with the experimental results. The Weibull modulus m and characteristic strength σ_0 used in these calculations are obtained from the Weibull plots of flexure tests as an average value of longitudinal and transverse samples. The volume dependence

of characteristic strength is also considered using the effective volume of the flexure sample and compression–torsion sample. The m and σ_0 for the compression–torsion sample are estimated to be 10.0 and 571 MPa for the as-machined sample, 13.5 and 694 MPa for the thermal-treated sample.

This analysis is based on the statistical theory of brittle fracture for volume-distributed flaws. As shown in Table 2 and Fig. 5, the lower tensile strength of as-machined samples at a low compressive stress state indicates the influence of surface condition. Therefore, the overall comparison between the theoretical strength envelope and experimental data is performed only on thermal-treated samples. The strength data have the inherent scatter caused by the brittle nature. The $\sigma_1^E(k) \pm 2\delta(k)$ show the 95% probability interval on the Weibull distribution for arbitrary k value. By comparing this 95% probability band to experimental results, the validity of strength prediction from statistical multiaxial fracture theory is evaluated.

The shear sensitivity constant C is reported to be varied in the range from 0.8 to 2.0 in the previous mixed-mode fracture tests performed on silicon nitride.[30,33–38] The calculated strength-envelopes using $C = 1.75$ for Shetty's criterion and $C = 1.65$ for the ellipsoidal criterion are drawn in Fig. 5 together with the 95% probability band for each envelope. The both predictions have little difference and include all experimental results of thermal-treated samples in the 95% probability band. This result shows that the strength behavior of thermal-treated silicon nitride is well described by the statistical multiaxial fracture theory, at least within the 95% probability band.

As mentioned above, only volume-distributed flaws are considered in this analysis. The discrepancy between the experimental results of the as-machined samples and predicted tensile strength indicates that the fracture behavior of the as-machined samples is more complicated because of a combined effect of surface and volume flaws at a low compressive stress state of $\sigma_3/\sigma_1 > -2.5$. However, in the high-compression stress state where $\sigma_3/\sigma_1 < -2.5$, the fracture strength of the as-machined sample corresponds to the experimental and theoretical strength for the thermal-treated samples, indicating that there are little differences of the fracture behavior between them. Therefore, it is expected that the fracture of the as-machined samples is dominated by the volume-distributed flaws under the high-compressive stress state.

The multiaxial fracture statistics predicts that tensile strength under a multiaxial stress state decreases because of the contribution of shear stress to a fracture. This tendency is verified by the thermal-treated samples. On the other hand, the as-machined samples show little weakening with increasing multiaxial stress. In the as-machined samples, the shear-stress-induced weakening is overlapped by decrease in strength due to the preexisting machining surface flaws. This competitive relation must be affected by material conditions and properties such as surface flaw conditions, internal defect structures, fracture toughness, shear sensitivity, and so on, and would cause the discrepancy of fracture behavior among previous studies.[6,8,9,11,13–17] The effect of thermal treatment has been observed even for as-machined samples polished using 2000 grit diamond paper in this study, indicating the strong severity of surface-condition-effects on tensile strength behavior under multiaxial loading.

5. Conclusion

In this study, the fracture behavior of silicon nitride under multiaxial stress state was investigated. The experiments were performed on the thermal treated and as-machined silicon nitride ceramics. In one-dimensional flexure tests, although the as-machined samples show strength anisotropy to the grinding direction, the thermal-treated samples shows considerable higher strengths with no grinding direction dependence. In the compression–torsion tests, the thermal-treated samples show considerably higher strength than the as-machined samples at low compressive stress states and weakening with increasing the compression stress. Under a highly compressive stress state, the strength of the thermal-treated samples is comparable to that of the as-machined sample. Although the fracture behavior of the thermal-treated samples is well described by the statistical theory of multiaxial fracture for volume-distributed flaws combined with empirical mixed-mode fracture criteria with the shear sensitivity constant of 1.75 and 1.65 for Shetty's criterion and the ellipsoidal criterion, respectively. The fracture behavior of the as-machined samples is expected to be controlled by complicated competing processes of surface and volume fracture. As a results, the thermal oxidation treatment of silicon nitride ceramics is useful not only for increasing in the tensile strength but also for better designing of ceramic components using the statistical fracture theory.

References

1. Lin HT, Ferber MK, Becher PF, Price JR, van Roode M, Kimmel JB, et al. Characterization of first-stage silicon nitride components after exposure to an industrial gas turbine. *Journal of the American Ceramic Society* 2006;**89**:258–65.
2. Motoyashiki Y, Hasegawa S, Okudaira K, Sato E. Micrometeoroid impact on ceramic thin components for interplanetary probe. *International Journal of Impact Engineering* 2008;**35**:1666–71.
3. Batdorf SB, Heinisch Jr HL. Weakest link theory reformulated for arbitrary fracture criterion. *Journal of the American Ceramic Society* 1978;**61**:355–8.
4. Evans AG. A general approach for the statistical analysis of multiaxial fracture. *Journal of the American Ceramic Society* 1978;**61**:302–8.
5. Matsuo Y. Probabilistic analysis of brittle fracture loci under bi-axial stress state. *Transactions of the Japan Society of Mechanical Engineering: A* 1980;**46**:605–12.
6. Broutman LJ, Krishnakumar SM, Mallick PK. Effects of combined stresses on fracture of alumina and graphite. *Journal of the American Ceramic Society* 1970;**53**:649–54.
7. Ely RE. Strength of titania and aluminum silicate under combined stresses. *Journal of the American Ceramic Society* 1972;**55**:347–50.
8. Oh KPL, Vardar Ö, Finnie I. Failure of brittle solids under biaxial stresses. *International Journal of Fracture* 1973;**9**:372–5.
9. Petrovic JJ, Stout MG. Fracture of Al_2O_3 in combined tension/torsion: I. Experiments. *Journal of the American Ceramic Society* 1981;**64**:656–60.
10. Petrovic JJ, Stout MG. Fracture of Al_2O_3 in combined tension/torsion: II. Weibull theory. *Journal of the American Ceramic Society* 1981;**64**:661–6.
11. Stout MG, Petrovic JJ. Multiaxial loading fracture of Al_2O_3 tubes: I. Experiments. *Journal of the American Ceramic Society* 1984;**67**:14–8.
12. Stout MG, Petrovic JJ. Multiaxial loading fracture of Al_2O_3 tubes: II. Weibull theory and analysis. *Journal of the American Ceramic Society* 1984;**67**:18–23.

13. Ikeda K, Igaki H. Fracture criterion for alumina ceramics subjected to triaxial stresses. *Journal of the American Ceramic Society* 1984;**67**:538–44.
14. Oda I, Matsui M, Soma T, Masuda M, Yamada N. Fracture behavior of sintered silicon nitride under multiaxial stress states. *Journal of the Ceramic Society of Japan* 1988;**96**:539–45.
15. Kim KT, Suh J. Fracture of alumina tubes under combined tension/torsion. *Journal of the American Ceramic Society* 1992;**75**:896–902.
16. Kokaji A, Uchimura H, Kaji M. Fracture strength of silicon nitride under biaxial stresses. *Journal of the Ceramic Society of Japan* 1992;**100**:1304–8.
17. Wang F, Lu M, Zheng X, Pan Y. Fracture of SiC tubes under combined tension/torsion. *International Journal of Fracture* 1996;**80**:49–54.
18. Zheng X, Zhao K, Wang H, Yan J. Failure criterion with given survivability for ceramic notched elements under combined tension/torsion. *Materials Science and Engineering: A* 2003;**357**:196–202.
19. Nohut S, Usbeck A, Özcoban H, Krause D, Schneider GA. Determination of the multiaxial failure criteria for alumina ceramics under tension–torsion test. *Journal of European Ceramic Society* 2010;**30**:3339–49.
20. Jakus K, Ritter JE, Rogers Jr WP. Strength of hot-pressed silicon nitride after high-temperature exposure. *Journal of the American Ceramic Society* 1984;**67**:471–5.
21. Choi SR, Tikare V. Crack healing behavior of hot pressed silicon nitride due to oxidation. *Scripta Metallurgica et Materialia* 1992;**26**:1263–8.
22. Ando A, Shirai Y, Nakatani M, Kobayashi Y, Sato S. (Crack-healing + proof test): a new methodology to guarantee the structural integrity of a ceramics component. *Journal of European Ceramic Society* 2002;**22**:121–8.
23. Houjou K, Ando K, Liu SP, Sato S. Crack-healing and oxidation behavior of silicon nitride ceramics. *Journal of European Ceramic Society* 2004;**24**:2329–38.
24. Dandekar DP, Casem DT, Motoyashiki Y, Sato E. Shock response of silicon nitride. In: Elert ML, Buttler WT, Furnish MD, Anderson WW, Proud WG, editors. *Shock compression of condensed matter—2009*. New York: AIP; 2009. p. 985–8.
25. ISO 20501:2003. Fine ceramics (advanced ceramics, advanced technical ceramics)—Weibull statistics for strength data.
26. Rice RW, Mecholsky JJ, Becher Jr PF. The effect of grinding direction on flow character and strength of single crystal and polycrystalline ceramics. *Journal of Materials Science* 1981;**16**:853–62.
27. Miyasato H, Okamoto H, Usui S, Miyamoto A, Ueno Y. The effect of grinding on strength of hot-pressed silicon nitride. *ISIJ International* 1989;**29**:726–33.
28. Strakna TJ, Jahanmir S, Allor RL, Kumar KV. Influence of grinding direction on fracture strength of silicon nitride. *Journal of Engineering Materials and Technology* 1996;**118**:335–42.
29. Danzer R, Lube T, Supancic P, Damani R. Fracture of ceramics. *Advanced Engineering Materials* 2008;**10**:275–98.
30. Shetty DK. Mixed-mode fracture criteria for reliability analysis and design with structural ceramics. *Journal of Engineering for Gas Turbines and Power* 1987;**109**:282–9.
31. Awaji H, Sato S. Combined mode fracture toughness measurement by the disk method. *Journal of Engineering Materials and Technology* 1978;**100**:175–82.
32. Lamon J, Evans AG. Statistical analysis of bending strengths for brittle solids: a multiaxial fracture problem. *Journal of the American Ceramic Society* 1983;**66**:177–82.
33. Petrovic JJ. Mixed-mode fracture of hot-pressed Si_3N_4. *Journal of the American Ceramic Society* 1985;**68**:348–55.
34. Koiso N, Misawa H, Kodama S. Fracture under mixed-mode loading in ceramics having a semi-circular crack. *Transactions of the Japan Society of Mechanical Engineering: A* 1989;**55**:1191–4.
35. Tsuruta H, Yamada N, Nakasuji Y, Masuda M, Matsui M. Fracture behavior of sintered silicon nitride under multiaxial stress states (part 2). *Journal of the Ceramic Society of Japan* 1991;**99**:574–81.
36. Tikare V, Choi SR. Combined mode I and mode II fracture of monolithic ceramics. *Journal of the American Ceramic Society* 1993;**76**:2265–72.
37. Ono T, Takenoshita T, Uchimura H, Kaji M. Fracture behavior of a silicon nitride ceramic under mixed-mode fracture condition. *Journal of the Ceramic Society of Japan* 1993;**101**:240–3.
38. Khandelwal P, Majumdar BS, Rosenfield AR. Mixed-mode high temperature toughness of silicon nitride. *Journal of Materials Science* 1995;**30**:395–8.